Available online at www.sciencedirect.com

ScienceDirect

Ceramics International 40 (2014) 1019–1027

CERAMICS INTERNATIONAL

www.elsevier.com/locate/ceramint

Preparation and electrochemical properties of spinel $LiFe_xCu_yMn_{1.2}O_4$ by ultrasonic spray pyrolysis

Burçak Ebin[a], Sebahattin Gürmen[a,*], Göran Lindbergh[b]

[a]Department of Metallurgical and Materials Engineering, Istanbul Technical University, 34469 Istanbul, Turkey
[b]Department of Chemical Engineering and Technology, Applied Electrochemistry, Royal Institute of Technology, KTH, SE-100 44 Stockholm, Sweden

Received 2 May 2013; received in revised form 25 June 2013; accepted 26 June 2013
Available online 10 July 2013

Abstract

Nanocrystalline $LiFe_xCu_yMn_{1.2}O_4$ (x and y=0.2, 0.4 and 0.6) particles were prepared by the ultrasonic spray pyrolysis method using nitrate salts at 800 °C in air atmosphere. Particle properties were characterized by X-ray diffraction, scanning electron microscopy, and energy dispersive spectroscopy. Also, cyclic voltammetry and galvanostatic tests were performed to investigate the effects of the double substituent and doping amounts on electrochemical behavior. Results show that the aggregation of nanocrystallites around 90 nm size formed submicron spherical cathode particles. Transition metal ratios in particles exhibited a perfect fit with desired amounts. Although the change of iron and copper amounts do not show significant differences in the particle size and shape morphology, they modify the 4 V and 3 V potential plateaus of spinel $LiMn_2O_4$. The discharge capacities of $LiFe_{0.2}Cu_{0.6}Mn_{1.2}O_4$ particles are 39 and 23 mAh g^{-1} for 4 and 2.6 V potential regions, respectively. 4 V discharge capacity disappeared with increasing of iron and decreasing of copper contents due to random occupation of iron and copper ions in the spinel lattice.

Keywords: Nanostructures; Cathode particles; Spinel structure; Li-ion batteries; Ultrasonic spray pyrolysis

1. Introduction

The use of Li-ion batteries arose because of growing demand in the light electronic market, and recently uncertainty of fossil fuels and increasing environmental concerns have triggered the development of hybrid and electronic vehicles powered by Li-ion batteries with high energy densities. Therefore, both scientific and industrial interest in Li-ion battery studies increased sharply in the last few years. Investigations to improve cathode materials are important lines of the research, because cathodes have a significant role in the properties of batteries [1–7]. Layered $LiCoO_2$, $LiNiO_2$ and spinel $LiMn_2O_4$ materials are commercially used as a Li-host material that permits insertion and deinsertion of Li^+ ions. However, their drawbacks are obstacles for future uses of Li-ion batteries [5–9]. Layered $LiCoO_2$ and $LiNiO_2$ have high capacity and good cycling performance, but their high cost, toxicity and safety problems limit their applications. $LiNiO_2$ has less stability and lower cation ordering, resulting in the nickel ions occupying lithium sites, which impedes Li^+ ions diffusion. Production of perfect layer $LiNiO_2$ structure has difficulties due to the lower degree of cation ordering [10–13]. The low cost, environmental friendly and excellent voltage profile features make the spinel $LiMn_2O_4$ favorable as a cathode material. However, $LiMn_2O_4$ exhibits unacceptable capacity fade during cycling performance due to phase changes, dissolution of manganese and asymmetric lattice expansion/contraction [13–16]. Despite the disadvantages of the spinel $LiMn_2O_4$, it is safer compared with layered oxides such as $LiCoO_2$ and $LiNiO_2$ which more easily combust with the electrolyte [17]. The electrochemical performance of spinels needs to be improved to use them in electrical vehicles.

Several studies were focused to advance the spinel $LiMn_2O_4$ features, and a series of metal (M: Co, Ni, Fe, Zn, Ti, Mg, Al, La, Ga and Nb) monodoped $LiM_xMn_{2-x}O_4$ structures have been prepared by various processes. This research showed that appropriate doping of elements increased the

*Correspondence to: Department of Metallurgical and Materials Engineering, Istanbul Technical University, Ayazaga Campus, 34469 Sarıyer, Istanbul, Turkey. Tel.: +90 212 285 68 62; fax: +90 212 285 34 27.
E-mail address: gurmen@itu.edu.tr (S. Gürmen).

0272-8842/$ - see front matter © 2013 Elsevier Ltd and Techna Group S.r.l. All rights reserved.
http://dx.doi.org/10.1016/j.ceramint.2013.06.099

cycling performance of lithium manganese oxide spinels, while worsening some electrochemical properties such as capacity [18–30]. Recently, bidoping has become a new trend to create better cathodes. Ooms et al. [31] reported that $LiMg_{\delta}Ni_{0.5-\delta}Mn_{1.5}O_4$ cathode particles prepared by a combination of sol–gel and solid-state processing exhibit improved cycling performance and rate capacity. He et al. [32] showed that 0.5% yttrium bulk doping, and 0.5% cobalt surface co-doping to $LiMn_2O_4$ is an effective way to enhance performance. Thirunakaran et al. [33] attempted to fabricate cerium and zinc dual-doping lithium manganese oxide spinel by sol–gel route using p-amino benzoic acid to raise the features of cathodes. Bi-cation substituted $LiCr_{0.2}V_{0.2}Mn_{1.6}O_4$ cathode synthesized via the citric acid assisted modified sol–gel method displayed a poor reversibility due to the ionic arrangement caused to lattice instability [34]. The electrochemical investigation of $LiNi_xCu_yMn_{2-x-y}O_4$ cathode particles prepared by the sol–gel method indicates that the capacity of spinel materials decreases with increasing doped Cu amount. However, copper doped spinel $LiCu_{0.25}Ni_{0.25}Mn_{1.5}O_4$ exhibits good rate capability due to the lower Li diffusion barrier and higher electronic conductivity of copper [35]. Although various studies performed to dual substitution of $LiMn_2O_4$, the suitable couple to improve characteristics of a bi-doped Li–Mn–O spinel system is still unclear.

Most of the methods in the literature to prepare dual-substituted lithium manganese oxide particles need expensive and environmentally unfriendly chemicals, and also include multi-steps. Furthermore, particle properties such as homogeneity, morphology and crystallinity directly depend on the fabrication method and strongly affect the electrochemical characteristics [36,37]. Ultrasonic spray pyrolysis (USP) is a versatile and simple technique to produce various materials in a wide range of composition, size and morphology. It is an easily controllable process to obtain particle in desired features. Particle preparation by the USP method involves four major steps: generation of the aerosol from corresponding solution, shrinkage of the droplets and precipitation due to evaporation of the solvent, decomposition/reduction reaction of the precursor and formation of primary particles (initially crystallites) and lastly densification. Thus, the final particles, generally in micrometer or sub-micrometer size, are the aggregates of the initial crystallites. The USP method is suitable for the production of metallic, alloy, oxide and composite particles in desired size range with homogeneous composition and dense or hollow morphologies [38–43].

In the past, expensive and toxic elements were partially substituted with Mn ions in the spinel structure. The present study focused on the preparation and understanding of electrochemical behaviors of bidoped lithium manganese oxide particles using iron and copper, which are low cost, highly abundant and non-toxic. This is the first ever attempt made to explore the electrochemical characteristics of Fe and Cu substituted spinel structure. Spinel $LiFe_xCu_yMn_{2-x}O_4$ (x and y=0.2, 0.4 and 0.6) particles were synthesized by the USP method. The particle characterization studies were performed as well as the electrochemical performance tests.

2. Experimental

Spinel $LiFe_xCu_yMn_{2-x}O_4$ (x and y=0.2, 0.4 and 0.6) particles were produced by the ultrasonic spray pyrolysis method. The precursor solutions were prepared by dissolving a stoichiometric amount of $LiNO_3$, $Mn(NO_3)_2 \cdot 4H_2O$, $Cu(NO_3)_2 \cdot 3H_2O$ and $Fe(NO_3)_3 \cdot 9H_2O$ (all from Merck™) in distilled water. Table 1 gives the ion concentrations of the precursor solution used in experiments. Tartaric acid solution was added to control the pH of the precursor solution and as an organic agent. The pH of the corresponding solutions was adjusted to 1.0. An ultrasonic nebulizer with a resonant frequency of 1.3 MHz (RBI-Instrumentation) was used to atomize the precursor solution. The aerosol stream was introduced into the horizontal quartz reactor at 800 °C by air flow. The quartz reactor was placed inside the tube furnace (Nabertherm, R 50/250/12) with a temperature control of ± 1 °C. The heated length and diameter of the quartz reactor are 250 and 20 mm, respectively. The flow rate of the air used as a carrier gas was fixed at 500 ml/min. The particles obtained by the decomposition of the metal nitrate aerosol droplets were collected in the washing bottles connected to the outlet of the quartz reactor.

X-ray diffraction (XRD, Phillips PW 1700) using Cu Kα radiation was used to examine the crystalline phase and size of the prepared particles. For data collection we continuously scanned a detector that covered an angular range from 10° to 90° with a step size of 0.0167 and wavelengths 1.541874 Å. The chemical compositions of particles were analyzed by an energy dispersive spectroscopy (EDS) instrument (Oxford/Inca). Particle size and morphology of the samples were investigated by field emission scanning electron microscopy (FE-SEM, JEOL JSM 700F).

Electrochemical analyses were performed using cycling voltammetry and charge–discharge tests on 2016 type coin cells. The cells were composed of a lithium metal negative electrode isolated from the positive electrode by a glass microfiber separator. 1 M $LiPF_6$ in ethylene carbonate:dimethyl carbonate

Table 1
Precursor concentrations for $LiFe_xCu_yMn_{1.2}O_4$ particles.

x	y	Concentration of $LiNO_3$ (M)	Concentration of $Mn(NO_3)_2 \cdot 4H_2O$ (M)	Concentration of $Fe(NO_3)_3 \cdot 9H_2O$ (M)	Concentration of $Cu(NO_3)_2 \cdot 3H_2O$ (M)
0.2	0.6	0.10	0.12	0.02	0.06
0.4	0.4	0.10	0.12	0.04	0.04
0.6	0.2	0.10	0.12	0.06	0.02

(EC:DMC, Merck™) was used as an electrolyte. The positive electrodes contained 70% $LiFe_xCu_yMn_{2-x}O_4$, 20% carbon black, and 10% polyvinylidene difluoride (PVDF) binder. These materials, which included 20 mg active cathode material were dispersed in 1-methyl-2pyrrolidione (NMP) and acetone, and then the resultant slurry was spread onto an aluminum foil using the doctor blade technique. The coated aluminum foil was dried in vacuum dryer at 80 °C for 12 h and then pressed to achieve a good adherence between the coated material and the aluminum foil. The coin cells were assembled inside a glove box filled with high purity argon gas. The cells were cycled galvanostatically between 2.2 and 4.8 V on battery tester (Solartron 1287 Potentiostat/Galvanostat) at 0.5 C charge–discharge rate. Cyclic voltammetry (CV) was performed between 2.2 and 4.8 V at scanning rate of 0.2 mV s^{-1} at room temperature.

3. Results and discussion

Fig. 1 shows XRD patterns of $LiFe_{0.2}Cu_{0.6}Mn_{1.2}O_4$, $LiFe_{0.6}Cu_{0.2}Mn_{1.2}O_4$ and $LiFe_{0.4}Cu_{0.4}Mn_{1.2}O_4$ particles produced by the USP method at 800 °C. All of the peaks in the XRD patterns correspond to the cubic spinel structure of $LiMn_2O_4$ with Fd-3m space group. The crystallographic data of the particles such as the crystallite size, lattice parameter and peak intensity ratios are shown in Table 2. The crystallite size of $LiFe_xCu_yMn_{1.6}O_4$ particles were determined by the Scherrer equation using (111), (311) and (400) diffraction lines in the XRD patterns. Instrumental broadening was taken into account to obtain accurate crystallite size in the calculation. The crystallite sizes of particles were almost the same and determined as 86, 95 and 84 nm by increasing iron and decreasing copper content. The changing of the doping elements (Fe and Cu) amount does not have a dominant effect on the crystallite size. Lattice parameters of the samples were obtained by the least squares method, and showed an elongation with the increasing of Fe and decreasing of Cu amounts. We expected shrinkage of the lattice with decreasing Cu due to its bigger ionic radius compared to Mn^{3+} and Fe^{3+} ($Cu^{2+}=87$ pm, $Fe^{3+}=63$ pm and $Mn^{3+}=72$ pm). However, occupation of the dopant cations into the 8a tetrahedral (Li^+ positions) or 16c octahedral sites in the structure instead of 16d octahedral sites may cause this surprising increase in the lattice parameter.

The integrated intensity ratios of the (400)/(311) and (220)/(311) peaks are indices of the extent of occupancy of the substituent ions. The change in the intensity ratio of (220)/(311) was opposite to that of (400)/(311); for instance the intensity ratio of (220)/(311) rises while that of (400)/(311) reduces when dopant ions at the 8a sites increased or those at the 16d sites decreased [44]. We used spinel $LiMn_2O_4$ (JCPDS Card no: 01-089-0106) XRD data, which is best fitted with the samples, to compare the intensity changes (Table 2). All the samples exhibit higher values for (220)/(311) peaks and lower values for (400)/(311) peaks than the reference. The results are consistent with Fe and Cu mono-doped Li–Mn–O spinels. In our previous works on $LiFe_xMn_{2-x}O_4$ [45] and $LiCu_xMn_{2-x}O_4$ [46] cathode particles, cationic distribution in the

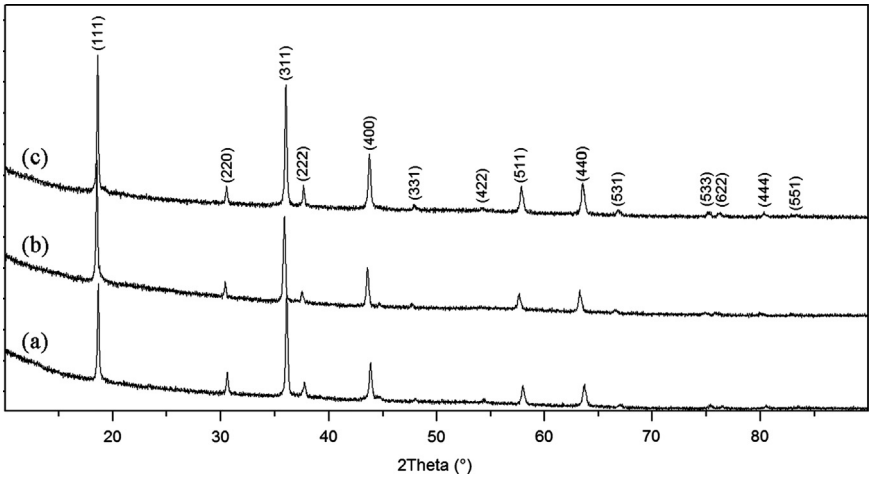

Fig. 1. XRD patterns of the samples (a) $LiFe_{0.2}Cu_{0.6}Mn_{1.2}O_4$, (b) $LiFe_{0.6}Cu_{0.2}Mn_{1.2}O_4$ and (c) $LiFe_{0.4}Cu_{0.4}Mn_{1.2}O_4$.

Table 2
Crystallite sizes, lattice parameters and integrated peak intensity ratios as a function of the substituent amount in $LiFe_xCu_yMn_{1.2}O_4$ particles.

x	y	Crsytallite size (nm)	Lattice parameter (Å)	$I(220)/I(311)$	$I(400)/I(311)$
0.2	0.6	86	8.247	0.203	0.359
0.4	0.4	95	8.269	0.146	0.461
0.6	0.2	84	8.303	0.166	0.441
$LiMn_2O_4$[a]			8.251	0.013	1.107

[a] $LiMn_2O_4$, JCPDS Card no: 01-089-0106.

spinel was changed by substitution of Fe or Cu, and increasing substitution amounts caused new phase formations. It is known that iron cations in spinel lithium iron oxide structure occupy both 8a tetrahedral and 16d octahedral sites where lithium ions occupy 16d octahedral sites [47]. Ohzuku et al. [44] reported that iron ions distributed at 8a tetrahedral and 16d octahedral sites in $LiFe_yMn_{2-y}O_4$ spinel for the situation $y > 0.57$. According to Arai et al. [48], lithium copper oxide structures (Li_2CuO_2, $Li_3Cu_2O_4$, and $LiCuO_2$) have one dimensional CuO_4 chains, where copper is the center of oxygen rectangle.

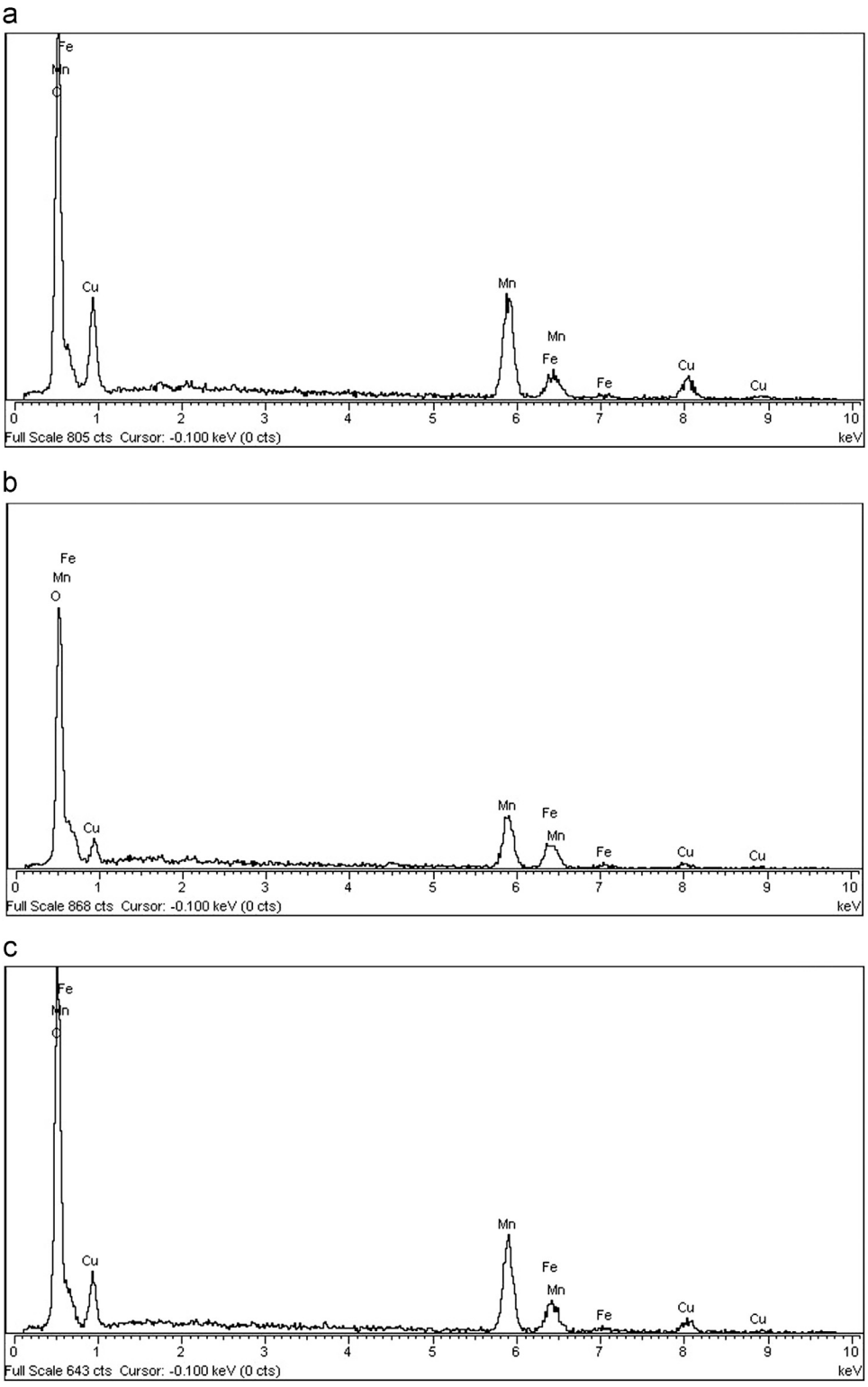

Fig. 2. EDS analysis of the samples (a) $LiFe_{0.2}Cu_{0.6}Mn_{1.2}O_4$, (b) $LiFe_{0.6}Cu_{0.2}Mn_{1.2}O_4$ and (c) $LiFe_{0.4}Cu_{0.4}Mn_{1.2}O_4$.

Moreover, the positioning of copper ions in the $LiMn_2O_4$ spinel structure is extremely complex leading to deficient incorporation of Cu in the structure due to the stability and low reactivity of copper oxide [49,50]. Evidently a high concentration of iron and copper in the spinel Li–Mn–O structure leads to a random occupation of doping ions in both tetrahedral and octahedral sites causing the lithium displacement and probably movement of Li^+ ions into the octahedral sites.

Table 3
Chemical contents of $LiFe_xCu_yMn_{1.2}O_4$ cathode particles.

x	y	Experimental Mn:Fe:Cu	Theoretical Mn:Fe:Cu
0.2	0.6	6.34:1:2.48	6:1:3
0.4	0.4	3.12:1.01:1	3:1:1
0.6	0.2	2:1:0.36	2:1:0.33

The stoichiometries of the synthesized cathode materials were investigated using EDS analysis (Fig. 2a–c), wherein the percentages of the individual elements have been confirmed, with an exception of Li. It is not possible to detect lithium by EDS due to the detection limit between B and U. Elemental content of the particles obtained by EDS are given in Table 3. EDS analysis showed that Mn:Fe:Cu ratio in the samples were close to desired value. However, $LiFe_{0.2}Cu_{0.6}Mn_{1.2}O_4$ particles have slightly lower Cu content than the desired value because of the lower stability and solid solubility of Cu at high amounts in spinel framework. Results indicates that particle composition is controllable in USP process by changing the ratio of the precursor salt concentrations, and also the USP process is a suitable method to produce homogeneous particles with complex compositions.

SEM images of the samples are shown in Fig. 3. The change of iron and copper dopings had almost no effect on the particle

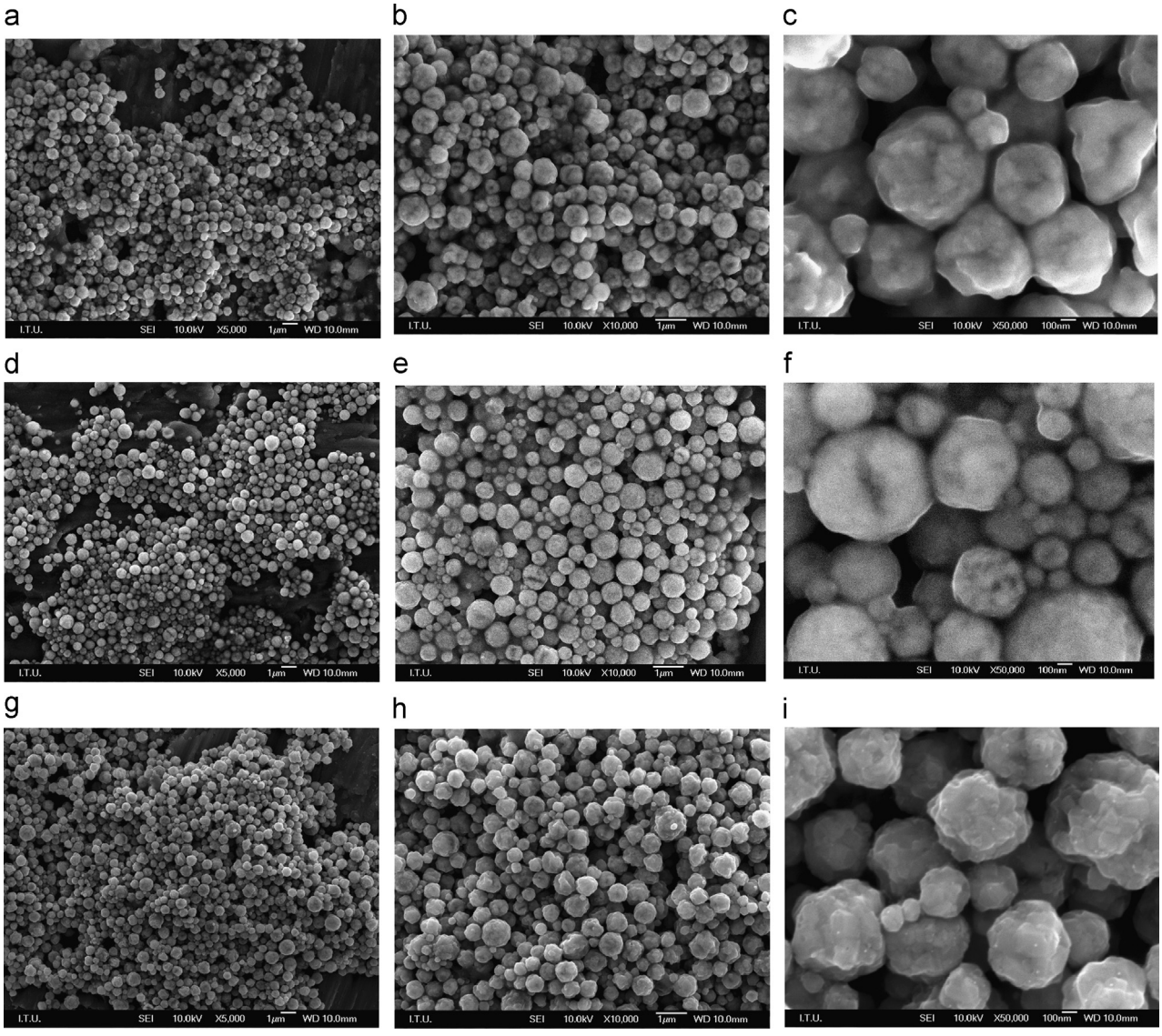

Fig. 3. SEM images of the samples (a) $LiFe_{0.2}Cu_{0.6}Mn_{1.2}O_4$, X5K, (b) $LiFe_{0.2}Cu_{0.6}Mn_{1.2}O_4$, X10K, (c) $LiFe_{0.2}Cu_{0.6}Mn_{1.2}O_4$, X50K, (d) $LiFe_{0.6}Cu_{0.2}Mn_{1.2}O_4$, X5K, (e) $LiFe_{0.6}Cu_{0.2}Mn_{1.2}O_4$, X10K, (f) $LiFe_{0.6}Cu_{0.2}Mn_{1.2}O_4$, X50K, (g) $LiFe_{0.4}Cu_{0.4}Mn_{1.2}O_4$, X5K (h), $LiFe_{0.4}Cu_{0.4}Mn_{1.2}O_4$, X10K, and (i) $LiFe_{0.4}Cu_{0.4}Mn_{1.2}O_4$, X50K.

size and shape morphology. All the particles have a spherical morphology with a particle size range between 80 nm and 1 μm and an average particle size about approximately 600–700 nm. In the USP process, particle formation begins with nucleation of the primary (nano-sized) particles, and then secondary submicron particles are obtained by aggregation of them. On magnified SEM images (Fig. 3c, f and i), primary particles on the secondary particle surfaces still can be observed and their sizes are compatible with the calculated crystallite sizes of the samples by the Scherrer equation. The reason for the existence of very fine particles is the instability of the droplets due to the reaction conditions such as collision of the droplets leading to break up of the primary particle clusters. Apparently, primary particles aggregated with just a few others and caused broader particle size distribution.

Fig. 4 exhibits the cycling voltammograms of the coin cells containing nanocrystalline $LiFe_xCu_yMn_{2-x}O_4$ (x and $y=0.2$, 0.4 and 0.6) spinel cathode particles versus lithium. All measurements were performed at room temperature in the voltage range of 2.2–4.8 V and at a scan rate 0.2 mV s^{-1}. It is known that the 4 V potential plateau exists due to Mn^{3+}/Mn^{4+} redox reactions taking place with two steps, while the extraction of Li^+ ions occurs by movement of 8a tetrahedral to 16 c octahedral sites. Excess Li^+ positioning in 16 c octahedral sites in $Li_xMn_2O_4$ ($1<x<2$) causes the 3 V potential plateau [26,28,51,52]. Moreover, a potential above 4.5 V can appear due to redox reactions of iron cations (Fe^{3+}/Fe^{4+}) that occupy 16d octahedral sites in the spinel Li–Fe–Mn–O structure [44,53]. On the other hand, Fe^{2+}/Fe^{3+} redox reaction for tetrahedral $LiFeO_2$ in the voltage range below 3.5 V [54]. The calculated voltage of the Cu^{2+}/Cu^{3+} redox couple is 4.44 V [35] and copper substituted spinels indicate high voltage output [55]. Results for $LiFe_{0.2}Cu_{0.6}Mn_{1.2}O_4$ particles show that the two oxidation peaks during charging at 3.15 V and 4.21 V correspond to two step Li^+ de-intercalation from the cathode. The two reduction peaks during discharging at 2.61 V and 3.93 V correspond to Li^+ intercalation into the cathode. The distinct separation of the peaks ($\Delta E_p=0.27$ for 3 V range and $\Delta E_p=0.14$ for 4 V range) and their symmetrical nature during both oxidation and reduction revealed the reversible/quasi-reversible characteristic of Li^+ in the $LiFe_{0.2}Cu_{0.6}Mn_{1.2}O_4$ cathodes. The nanocrystalline $LiFe_{0.6}Cu_{0.2}Mn_{1.2}O_4$ cathode displays two oxidation peaks at 3.13 V and 4.11 V values, but one reduction peak at 2.63 V. Likewise, two small anodic peaks at 3.13 V and 4.18 V, and one weak cathodic peak at 2.68 V are observed from CV result of $LiFe_{0.4}Cu_{0.4}Mn_{1.2}O_4$ cathode particles.

Discharge curves of the nanocrystalline spinel particles are presented in Fig. 5. Samples were charged to 4.8 V followed by discharging to 2.2 V at 0.5 C rate. Discharge capacity curves are compatible with the CV curves. $LiFe_{0.2}Cu_{0.6}Mn_{1.2}O_4$ particles displayed 39 mAh g^{-1} discharge capacity at 4 V region (4.8–3.0 V) and 23 mAh g^{-1} capacity at 2.6 V region (3.0–2.2 V). The

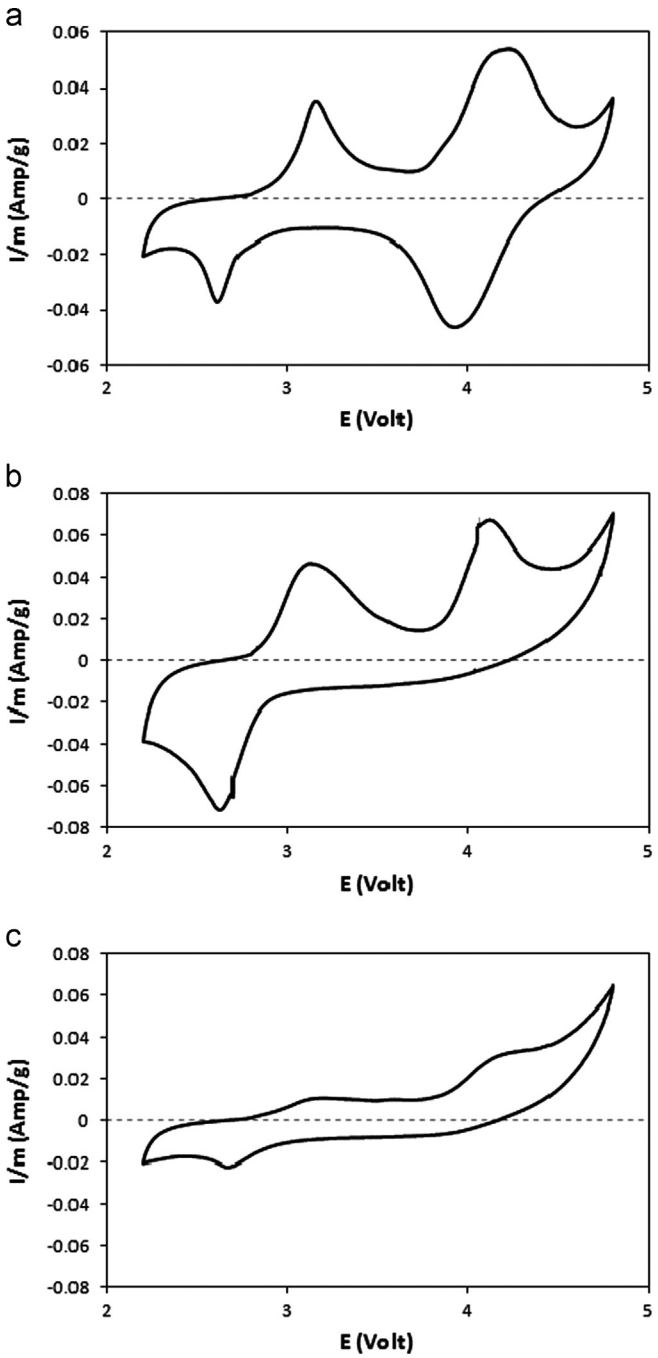

Fig. 4. Cyclic voltammograms of (a) $LiFe_{0.2}Cu_{0.6}Mn_{1.2}O_4$, (b) $LiFe_{0.6}Cu_{0.2}Mn_{1.2}O_4$ and (c) $LiFe_{0.4}Cu_{0.4}Mn_{1.2}O_4$.

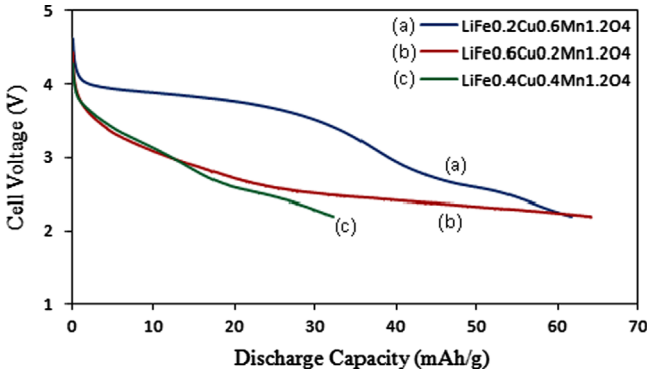

Fig. 5. First cycle discharge curves of samples. Cycling conditions: 2.2–4.8 V @ 0.5 C rate.

cumulative capacity is 62 mAh g^{-1} at 4.8–2.2 V potential region. 4 V capacity clearly belongs to Mn^{3+}/Mn^{4+} redox couple. The discharge potential of $LiFe_{0.6}Cu_{0.2}Mn_{1.2}O_4$ sample decreased rapidly below 4 V and showed a potential plateau around 2.6 V with 64 mAh g^{-1} discharge capacity. In this sample, high amount of iron and low amount of copper contents caused shifting of the discharge potential to lower voltage values by the effect of Fe^{2+}/Fe^{3+} couple. The discharge capacity curve of $LiFe_{0.4}Cu_{0.4}Mn_{1.2}O_4$ particles showed nearly same behavior above 3 V with $LiFe_{0.6}Cu_{0.2}Mn_{1.2}O_4$ particles, but reduced more sharply with the cell potential below 3 V. Bakenov et al. [56] stated that $LiMn_2O_4$ cathode particles produced by the USP method at 800 °C have nearly 120 mAh g^{-1} discharge capacity at 4 V range. Park et al. [57] produced nanocrystalline $LiMn_2O_4$ particles by the USP method and their discharge capacities were 80 and 125 mAh g^{-1} on the 4 V and 3 V potential ranges, respectively. According to these results, nanocrystalline $LiFe_xCu_yMn_{1.2}O_4$ cathode particles exhibited reduced discharge capacity comparing to spinel $LiMn_2O_4$ particles. Similar results observed in monodoped $LiM_xMn_{2-x}O_4$ (M = Fe and Cu) studies [45,46,50,55,58].

In spite of testing samples between 4.8 V and 2.2 V potential range, the inception of a high voltage plateau corresponding to Fe^{3+}/Fe^{4+} did not appear. However Fe^{2+}/Fe^{3+} redox couple occurs between 3.5 and 2.0 V potential range [54], and also voltage profile between 3.6 and 2.0 V corresponds to Cu^{1+}/Cu^{2+} redox couple [59]. Thus, potential profiles of $LiFe_xCu_yMn_{1.2}O_4$ cathodes originate Fe^{2+}/Fe^{3} and Cu^{1+}/Cu^{2+} redox couples, as well as Mn^{3+}/Mn^{4+} redox couple. Electrochemical test results showed that high amount dual substitution of iron and copper caused the disappearance of capacity at the 4 V region, and reduced the capacity at the 3 V region of spinel $LiMn_2O_4$ to 2.6 V. Possible reasons for the change of the electrochemical properties of dual substituted cathodes are not only reducing concentration of active Mn^{3+} cations in the structure, but also cationic rearrangement due to the complex distribution of iron and copper cations. Accordingly, we consider that copper ions are instable in cubic $LiFe_xCu_yMn_{2-x}O_4$ structure. They could replace the neighboring vacant 16c octahedral and 8a tetrahedral sites during the electrochemical reaction and limited the Li^+ insertion/extraction, which diffuse in the 8a → 16c → 8a path through the spinel structure. Hence we suggest that iron ions are irreversibly located in the 8a tetrahedral sites during charging in $LiFe_xCu_yMn_{1.2}O_4$ cathode particles. Rearrangement of doping cations changed oxidation states of Mn and also prevent the Li^+ insertion in 8a tetrahedral positions, resulting in the disappearance of 4 V discharge region, observed in $LiFe_{0.6}Cu_{0.2}Mn_{1.2}O_4$ and $LiFe_{0.4}Cu_{0.4}Mn_{1.2}O_4$ particles.

4. Conclusion

Spinel $LiFe_{0.2}Cu_{0.6}Mn_{1.2}O_4$, $LiFe_{0.6}Cu_{0.2}Mn_{1.2}O_4$ and $LiFe_{0.4}Cu_{0.4}Mn_{1.2}O_4$ particles have been successfully prepared by the ultrasonic spray pyrolysis method. Spherical shape submicron size particles were formed by aggregation of the nanoparticles. Compatible transition metals content in the particles with the desired chemical composition in the experiments shows that the USP method enabled the production of complex oxide particles composed of nanocrystallites. Ratios of iron and copper substitutions affected the electrochemical characteristic of cathode particles. The existence of high amount of iron in the spinel structure with a small amount of copper directly eliminated the 4 V capacity and low potential capacity has been dominate. Also, 10% iron and 30% copper atomic substitutions reduced both 2.6 and 4 V discharge capacities of pure spinel $LiMn_2O_4$ due to complex cation ordering as well as reducing concentration of electrochemically active Mn^{3+} ions.

Acknowledgments

This research was supported by Istanbul Technical University Research Fund (ITU-BAP). We would like to thank the Tinçel Culture Foundation that provided research fellowships for Burçak Ebin allowing 5 months stay at the KTH- Royal Institute of Technology, Applied Electrochemistry. Authors also thank Prof. Dr. Gültekin Göller and Technician Hüseyin Sezer for SEM characterizations.

References

[1] D. Choi, P.N. Kumta, Surfactant base sol–gel approach to nanostructured $LiFePO_4$ for high rate Li-ion batteries, J. Power Sources 163 (2007) 1064–1069.
[2] G. Meligrana, C. Gerbaldi, A. Tuel, S. Bodoardo, N. Penazzi, Hydrothermal synthesis of high surface $LiFePO_4$ powders as cathode for Li-ion cells, J. Power Sources 160 (2006) 516–522.
[3] Y. Wang, G. Cao, Developments in nanostructured cathode materials for high-performance lithium-ion batteries, Adv. Mater. 20 (2008) 2251–2269.
[4] H. Liu, Y.P. Wu, E. Rahm, R. Holze, H.Q. Wu, Cathode materials for lithium ion batteries prepared by sol–gel methods, J. Solid State Electrochem. 8 (2004) 450–466.
[5] H.-M. Xie, R.-S. Wang, J.-R. Ying, L.-Y. Zhang, A.F. Jalbout, H.-Y. Yu, G.-L. Yang, X.-M. Pan, Z.-M. Su, Optimized $LiFePO_4$-polyacene cathode material for lithium-ion batteries, Adv. Mater. 18 (2006) 2609–2613.
[6] A. Yamada, S.C. Chung, K. Hinokuma, Optimized $LiFePO_4$ for lithium battery cathode, J. Electrochem. Soc. 148 (3) (2001) A224–A229.
[7] N.-H. Kwon, T. Drezen, I. Exnar, I. Teerlinck, M. Isono, M. Graetzel, Enhanced electrochemical performance of mesoparticulate $LiMnPO_4$ for lithium ion batteries, J. Solid State Electrochem. 9 (6) (2006) A277–A280.
[8] C.H. Mi, X.B. Zhao, G.S. Cao, J.P. Tu, In situ synthesis and properties of carbon-coated $LiFePO_4$ as Li-ion battery cathodes, J. Electrochem. Soc. 152 (3) (2005) A483–A487.
[9] S. Komaba, S.-T. Myung, N. Kumagai, T. Kanouchi, K. Oikawa, T. Kamiyama, Hydrothermal synthesis of high crystalline orthorhombic $LiMnO_2$ as a cathode material for Li-ion batteries, Solid State Ionics 152–153 (2002) 311–318.
[10] Y. Chen, Y. Zhao, X. An, J. Liu, Y. Dong, L. Chen, Preparation and electrochemical performance studies on Cr-doped $Li_3V_2(PO_4)_3$ as cathode materials for lithium ion batteries, Electrochim. Acta 54 (2009) 5844–5850.
[11] J.T. Son, K.S. Park, H.G. Kim, H.T. Chung, Surface-modification of $LiMn_2O_4$ a with silver-metal coating, J. Power Sources 126 (2004) 182–185.
[12] L. Wang, J. Li, X. He, W. Pu, C. Wan, C Jiang, Recent advances in layered $LiNi_xCo_yMn_{1-x-y}O_2$ cathode materials for lithium ion batteries, J. Solid State Electrochem. 13 (2009) 1157–1164.
[13] J.W. Fergus, Recent developments in cathode materials for lithium ion batteries, J. Power Sources 195 (2010) 939–954.

[14] X. Li, F. Cheng, B. Guo, J. Chen, Template-synthesized $LiCoO_2$, $LiMn_2O_4$ and $LiNi_{0.8}Co_{0.2}O_2$ nanotubes as the cathode materials of lithium ion batteries, J. Phys. Chem. B 109 (2005) 14017–14024.
[15] D.K. Kim, P. Muralidharan, H.-W. Lee, R. Ruffo, Y. Yang, C.K. Chan, H. Peng, R.A. Huggings, Y. Cui, Spinel $LiMn_2O_4$ nanorods as lithium ion battery cathodes, Nano Lett. 8 (11) (2008) 3948–3952.
[16] N. Treuil, C. Labrugere, M. Menetrier, J. Portier, G. Campet, A. Deshayes, J.-C. Frison, S.-J. Hwang, S.-W. Song, J.-H. Choy, Relationship between chemical bonding nature and electrochemical property of $LiMn_2O_4$ spinel oxides with various particle sizes: electrochemical grafting concept, J. Phys. Chem. B 103 (1999) 2100–2106.
[17] B. Ammundsen, J. Paulsen, Novel lithium-ion cathode materials based on layered manganese oxides, Adv. Mater. 13 (2001) 943–956.
[18] D. Zhang, B.N. Popov, R.E. White, Electrochemical investigation of $CrO_{2.65}$ doped $LiMn_2O_4$ cathode materials for Li-ion batteries, J. Power Sources 76 (1998) 81–90.
[19] R.S. Liu, C.H. Shen, Structural and electrochemical study of cobalt doped $LiMn_2O_4$ spinels, Solid State Ionics 157 (2003) 95–100.
[20] Y.S. Lee, Y.K. Sun, S. Ota, T. Miyashita, M. Yoshio, Preparation and characterization of nano-crystalline $LiNi_{0.5}Mn_{1.5}O_4$ for 5 V cathode material by composite carbonate process, Electrochem. Commun. 4 (2002) 989–994.
[21] L. Zhang, X. Lv, Y. Wen, F. Wang, H. Su, Carbon combustion synthesis of $LiNi_{0.5}Mn_{1.5}O_4$ and its use as a cathode material for lithium ion batteries, J. Alloy. Compd. 480 (2009) 802–805.
[22] J.H. Kim, S.-T. Myung, Y.-K. Sun, Molten salt synthesis of $LiNi_{0.5}Mn_{1.5}O_4$ spinel for 5 V class cathode material of Li-ion secondary battery, Electrochim. Acta 49 (2004) 219–227.
[23] H.J. Bang, V.S. Donepudi, J. Prakash, Preparation and characterization of partially substituted $LiM_yMn_{2-y}O_4$ (M=Ni, Co, Fe) spinel cathodes for Li-ion batteries, Electochim. Acta 48 (2002) 443–451.
[24] R. Thirunakaran, A. Sivashanmugam, S. Gopukumar, C.D. Dunnill, D.H. Gregory, Studies on chromium/aluminum-doped manganese spinel as cathode materials for lithium ion batteries—a novel chelated sol–gel synthesis, J. Mater. Process. Tech. 208 (2008) 520–531.
[25] W. Cho, W. Ra, J. Shirakawa, M. Nakayama, M. Wakihara, Synthesis and electrochemical properties of nonstoichiometric $LiAl_xMn_{2-x}O_{4-\delta}$ as cathode materials for rechargeable lithium ion batteries, J. Solid State Chem. 179 (2006) 3534–3540.
[26] S.T. Yang, J.H. Jia, L. Ding, M.C. Zhang, Studies of structure and cycleability of $LiMn_2O_4$ and $LiNd_{0.01}Mn_{1.99}O_4$ as cathode for Li-ion batteries, Electrochim. Acta 48 (2003) 569–573.
[27] R. Singhal, S.R. Das, M.S Tomar, O. Ovideo, S. Nieto, R.E. Melgarejo, R.S. Katiyar, Synthesis and characterization of Nd doped $LiMn_2O_4$ cathode for Li-ion rechargeable batteries, J. Power Sources 164 (2007) 857–861.
[28] J. Tu, X.B. Zhao, D.G. Zhuang, G.S. Cao, T.J. Zhu, J.P. Tu, Studies of cycleability of $LiMn_2O_4$ and $LiLa_{0.01}Mn_{1.99}O_4$ as cathode materials for Li-ion battery, Physica B 382 (2006) 129–134.
[29] D. Arumugam, G.P. Kalaignan, K. Vediappan, C.W. Lee, Synthesis and electrochemical characterization of nano-scaled ZnO doped $LiMn_2O_4$ cathode materials for rechargeable lithium ion batteries, Electrochim. Acta 55 (2010) 8439–8444.
[30] C. Bellitto, E.M. Bauer, G. Righini, M.A. Green, W.R. Branford, A. Antonini, M. Pasquali, The effects of doping $LiMn_2O_4$ spinel on its use as a cathode in Li-ion batteries: neutron diffraction and electrochemical studies, J. Phys. Chem. Solid 65 (2004) 29–37.
[31] F.G.B. Ooms, E.M. Kelder, J. Schoonman, M. Wagemaker, F.M. Mulder, High-voltage $LiMg_8Ni_{0.5-\delta}Mn_{1.5}O_4$ spinels for Li-ion batteries, Solid State Ionics 152–153 (2002) 143–153.
[32] X. He, J. Li, Y. Cai, Y. Wang, J. Ying, C. Jiang, C. Wan, Preparation of co-doped spherical spinel $LiMn_2O_4$ as cathode materials for Li-ion batteries, J. Power Sources 150 (2005) 216–222.
[33] R. Thirunakaran, A. Sivashanmugam, S. Gopukumar, R. Rajalakshmi, Cerium and zinc: dual-doped $LiMn_2O_4$ spinels as cathode material for use in lithium rechargeable batteries, J. Power Sources 187 (2009) 565–574.
[34] N. Jayaprakash, N. Kalaiselvi, Gangulibabu, D. Bhuvaneswari, Effect of mono-(Cr) and bication (Cr,V) substitution on $LiMn_2O_4$ spinel cathodes, J. Solid State Electrochem. 15 (2011) 1243–1251.
[35] M.-C. Yang, B. Xu, J.-H. Cheng, C.-J. Pan, B.-J. Hwang, Y.S. Meng, Electronic, structural, and electrochemical properties of $LiNi_xCu_yMn_{2-x-y}O_4$ ($0<x<0.5$, $0<y<0.5$) high voltage spinel materials, Chem. Mater. 23 (2011) 2832–2841.
[36] I. Taniguchi, K. Matsuda, H. Furubayashi, S. Nakajima, Preparation of $LiMn_2O_4$ powders via spray pyrolysis and fluidized bed hybrid system, AIChE J. 52 (2006) 2413–2421.
[37] X. He, J. Li, Y. Cai, C. Jiang, C. Wan, Preparation of spherical spinel $LiMn_2O_4$ cathode material for Li-ion batteries, Mater. Chem. Phys. 95 (2006) 105–108.
[38] S. Gürmen, B. Ebin, S. Stopic, B. Friedrich, Nanocrystalline spherical iron-nickel (Fe–Ni) alloy particles prepared by ultrasonic spray pyrolysis and hydrogen reduction (USP-HR), J. Alloy. Compd. 480 (2009) 529–533.
[39] S. Gürmen, B. Ebin, Production and characterization of the nanostructured hollow iron oxide spheres and nanoparticles by aerosol route, J. Alloy. Compd. 492 (2010) 585–589.
[40] B. Ebin, S. Gürmen, C. Arslan, Synthesis and structural characterization of $LiZn_{0.5}Mn_{1.5}O_4$ cathode materials, Int. J. Mater. Sci. Electron. Res. 1 (2) (2010) 49–53.
[41] B. Ebin, S. Gürmen, Aerosol synthesis of nano-crystalline iron particles from iron (II) chloride solution, Metall-Forsch. 65 (4) (2011) 151–154.
[42] B. Ebin, S. Gürmen, Sythesis and characterization of nickel particles by hydrogen reduction assisted ultrasonic spray pyrolysis (USP-HR) method, KONA Powder Part. J. 29 (2011) 134–140.
[43] T.-H. Teng, M.-R. Yang, S.-H. Wu, Y.-P. Chiang, Electrochemical properties of $LiFe_{0.9}Mg_{0.1}PO_4$/carbon cathode materials prepared by ultrasonic spray pyrolysis, Solid State Commun. 142 (2007) 389–392.
[44] T. Ohzuku, K. Ariyoshi, S. Takedo, Y. Sakai, Synthesis and characterization of 5 V insertion material of $Li[Fe_yMn_{2-y}]O_4$ for lithium-ion batteries, Electrochim. Acta 46 (2001) 2327–2336.
[45] B. Ebin, S. Gürmen, C. Arslan, G. Lindbergh, Electrochemical properties of nanocrystalline $LiFe_xMn_{2-x}O_4$ ($x=0.2-1.0$) cathode particles prepared by ultrasonic spray pyrolysis method, Electrochim. Acta 76 (2012) 368–374.
[46] B. Ebin, S. Gürmen, G. Lindbergh, Electrochemical properties of nanocrystalline $LiCu_xMn_{2-x}O_4$ ($x=0.2$–0.6) cathode particles prepared by ultrasonic spray pyrolysis method, Mater. Chem. Phys. 136 (2012) 424–430.
[47] M.M. Thackeray, Spinel electrodes for lithium batteries, J. Am. Ceram. Soc. 82 (12) (1999) 3347–3354.
[48] H. Arai, S. Okada, Y. Sakurai, J.-I. Yamaki, Electrochemical and structural study of Li_2CuO, $LiCuO_2$ and $NaCuO_2$, Solid State Ionics 106 (1998) 45–53.
[49] G.T.-K. Fey, C.-Z. Lu, T.P. Kumar, Preparation and electrochemical properties of high-voltage cathode materials, $LiM_yNi_{0.5-y}Mn_{1.5}O_4$ (M=Fe, Cu, Al, Mg; $y=0.0-0.4$), J. Power Sources 115 (2003) 332–345.
[50] R. Thirunakaran, B.-R. Babu, N. Kalaiselvi, P. Periasamy, T.P. Kumar, N.G. Renganathan, M. Raghavan, N. Muniyandi, Electrochemical behaivour of $LiM_yMn_{2-y}O_4$ (M=Cu, Cr; $0\leq y\leq 0.4$), Bull. Mater. Sci. 24 (1) (2001) 51–55.
[51] S.-H. Kang, J.B. Goodenough, L.K. Rabenberg, Effect of ball-milling on 3 V capacity of lithium-manganese oxospinel cathodes, Chem. Mater. 13 (2001) 1758–1764.
[52] M. Wakihara, H. Ikuta, Y. Uchimoto, Structural stability in partially substituted lithium manganese spinel oxide cathode, Ionics 8 (2002) 329–338.
[53] H. Kawai, M. Nagata, M. Tabuchi, H. Tukamoto, R.A. West, Novel 5 V spinel cathode $Li_2FeMn_3O_8$ for lithium ion batteries, Chem. Mater. 10 (1998) 3266–3268.
[54] A.R. Armstrong, D.W. Tee, F.L. Mantia, P. Novak, P.G. Bruce, Synthesis of tetrahedral $LiFeO_2$ and its behavior as a cathode in rechargeable lithium batteries, J. Am. Chem. Soc. 130 (2008) 3554–3559.
[55] K.R. Murali, T. Saravanan, M. Jayachandran, Synthesis and characterization of copper substituted lithium manganete spinels, J. Mater. Sci: Mater. Electron. 19 (2008) 533–537.

[56] Z. Bakenov, M. Wakihara, I. Taniguchi, Battery performance of nanostructured lithium manganese oxide synthesized by ultrasonic spray pyrolysis at elevated temperature, J. Solid State Electrochem. 12 (2008) 57–62.

[57] S.-H. Park, S.-T. Myung, S.-W. Oh, C.-S. Yoon, Y.-K. Sun, Ultrasonic spray pyrolysis of nano crystalline spinel $LiMn_2O_4$ showing good cycling performance in the 3 V range, Electrochim. Acta 51 (2006) 4089–4095.

[58] I. Taniguchi, Z. Bakenov, Spray pyrolysis synthesis of nanostructured $LiFe_xMn_{2-x}O_4$ cathode materials for lithium-ion batteries, Powder Technol. 159 (2005) 55–62.

[59] T. Li, X.P. Ai, H.X. Yang, Reversible electrochemical conversion reaction of Li_2O/CuO nanocomposites and their applications as high-capacity cathode materials for Li-ion batteries, J. Phys. Chem. C 115 (2011) 6167–6174.